PUBLICATIONS OF THE ASTRONOMICAL SOCIETY OF THE PACIFIC
101: 832–838, September 1989

THE MORPHOLOGY OF REVERSED SPECTRAL-LINE BISECTORS

DAVID F. GRAY

Department of Astronomy, University of Western Ontario, London, ON N6A 3K7, Canada

Received 1989 April 15, revised 1989 June 9

ABSTRACT

Spectral-line asymmetries of stars on the hot side of the granulation boundary in the H-R diagram are contrasted with those on the cool side by comparing the line bisectors of 41 Cyg to those of α CMi. The reversed line bisectors for stars on the hot side of the boundary are interpreted to indicate large upward-stream velocities, ~ -10 to -20 km s^{-1}, over a small time-averaged fraction of the surface, $\approx 10\%$. Scaling properties of the bisectors imply no differential velocities within the up-flow.

Key words: spectroscopy–stellar atmospheres–convection

1. Introduction

Small asymmetries of spectral-line profiles in cool stars are generally attributed to granulation-type velocity fields in which rising gases are hotter and brighter than the falling gases. This explicit correlation between velocity and the fraction of light contributed to the observed spectrum is the fundamental reason for the *asymmetric* distribution of Doppler shifts shaping these stellar line profiles. The tool most frequently used to describe the asymmetry is the line bisector. One constructs the bisector of a line by finding the locus of midpoints of horizontal line segments running between the sides of the profile. Line bisectors are sensitive to several physical parameters of the photospheric dynamics, and a careful measurement and interpretation of bisector shapes allows these phenomena to be studied. More specifically, this is one of the few direct observational connections with stellar convection, that complex phenomenon affecting numerous areas of stellar physics, including basic energy transport, acoustic waves, magnetic fields and dynamo activity, Alfven waves, the support of chromospheres and corona, angular momentum redistribution within stars, the possible regulation of stellar rotation, Li depletion, and so on.

Customarily we think of photospheric velocity fields such as granulation as something natural to cool stars and cool stars only. This general misconception arises because we associate granulation with convective envelopes which in cool stars form an integral part of the energy transport. But these convective envelopes are the *deep* convective envelopes, significant in the context of stellar interiors, where the surface transition region is little more than a mathematical boundary and of small consequence in determining the stellar structure. In contrast, if one considers instead the surface layers in their own right, then the evidence is strongly in favor of significant, even large, velocities in the photospheres of hot stars. Mixing-length calculations, for example, predict high velocities even though the convection zone is superficial from the stellar-interiors point of view (e.g., Cox and Giuli 1968; Renzini *et al.* 1977). The observations tell a similar story. Spectral line broadening increases monotonically toward hotter stars at least up to late A stars (Gray 1988; Gray and Cheng 1989), and line bisectors of hotter stars are also most easily interpreted in terms of large velocities, as we shall see below.

Classical bisectors, reflecting solar-like granulation, are shaped somewhat like a distorted letter "C" (Voigt 1956, 1959; Schroter 1957; Dravins 1982; Rutten and Severino 1989) or, for stars somewhat hotter or more luminous than the Sun, like the top half of a "C" (Gray 1982; Dravins 1989). The extent of the bisector in wavelength, called the velocity span, decreases monotonically along the main sequence, ranging from $\sim$ 600–700 m s^{-1} for F dwarfs to less than $\sim$ 70 m s^{-1} for K dwarfs (Gray 1988). Recently we have discovered that stars hotter than a "granulation boundary" in the H-R diagram show bisectors of *reversed curvature* (Gray and Nagel 1989). This boundary runs from G1 I*b* to near F0 on the main sequence. Stars on the hot side of this line will be referred to as "hot stars" and those on the cool side as "cool stars". The bisectors for hot stars differ dramatically from those for cool stars, and the implications for photospheric velocity fields may be equally dramatic. The shape and various other characteristics of reversed bisectors are unlike anything seen for cool stars. Notably, the slope and curvature are opposite the classical case and the velocity span is several times larger, reaching values as high as 2000–3000 m s^{-1}. As a first step toward understanding these reversed bisectors, I make a comparison here between the morphology of the two types of bisectors.

2. Observational Data

I selected 41 Cygni and α Canis Minoris as representatives of the hot and cool stars, respectively. Figure 1 shows the position of these stars relative to the granulation boundary. The main reason these particular stars were chosen is their apparent brightness, a factor of basic importance in obtaining high signal-to-noise ratios in the recorded line profiles. Although the chosen stars differ substantially in surface gravity, it is nevertheless true that each represents the essential features of stars on opposite sides of the granulation boundary. Table 1 lists the exposures obtained for this investigation. They were made using the 1.2-m telescope at the University of Western Ontario. The coudé spectrograph and the 1872-diode Reticon detector give a field of about 65 Å in the 9th order with a resolution of ~ 3.5 km s^{-1} (Gray 1986*a*). Numerical experiments show that for bisector work it is not advantageous to remove the instrumental profile.

Two spectral regions were used, one centered near λ6150, the other near λ6250. Line blending is always a problem. Experience has shown that three lines in the first region (Ca I λ6122.23, Ba II λ6141.72, Ca I λ6162.18) and four lines in the second region (Fe I λ6230.74, Fe I λ6232.65, Fe I λ6252.57, Fe I λ6265.14) are sufficiently unblended and suitable for the study of reversed bisectors. (A few additional lines can be used for α CMi because the line blending is less severe.) These lines span a wide range in equivalent width, from 48 mÅ to 304 mÅ for 41 Cyg and from 20 mÅ to 155 mÅ for α CMi.

Prior to construction of the bisectors, the high-frequency noise was removed using an analytical version of the optimum noise filter (Gray 1976). Each line bisector was then constructed by finding midpoints of horizontal lines running from each measured point on the left-hand side of the profile to an interpolated point on the right-hand side. A cubic spline routine based on the one published by Hill (1982) was used. In addition, the number of bisector points was doubled by repeating the process for interpolated points on the left-hand side of the profile.

TABLE 1

The Observations

Star	B-V	Sp	Date	λ,Å	S/N
α C Mi	0.42	F5 IV-V	30MY88	6150	680
			28MY88	6150	600
			11MY88	6150	730
			24AP88	6250	810
			22AP88	6250	730
			11AP88	6250	770
			10AP88	6250	890
			08AP88	6250	800
			17AP87	6250	520
			23AP86	6150	680
			23AP86	6150	890
			23AP86	6150	680
			22AP86	6250	630
			02OC85	6150	760
			02OC85	6150	850
			02OC85	6150	880
41 Cyg	0.40	F5 II	09SE88	6250	750
			07SE88	6150	650
			25OC87	6250	560
			13OC87	6250	580
			04OC87	6150	690
			04OC87	6250	530
			27SE87	6150	560
			27SE87	6250	570
			26SE87	6250	580
			28JN87	6150	440
			06OC84	6250	310
			05OC84	6250	110
			18JN84	6250	200

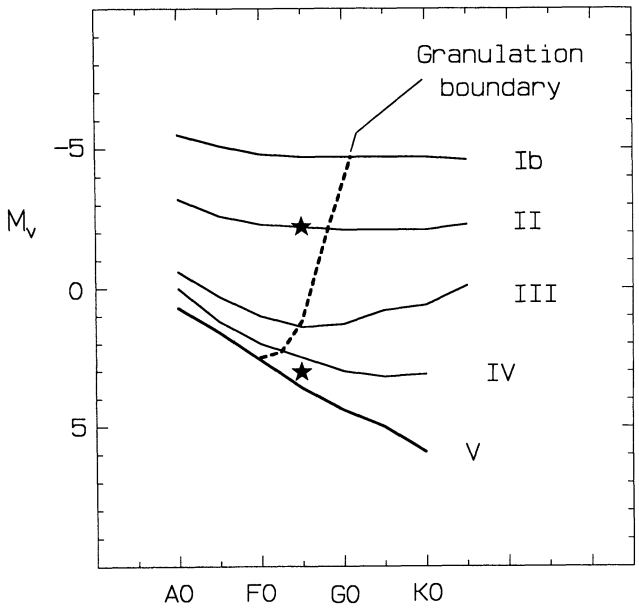

FIG. 1–The program stars are chosen to be on opposite sides of the granulation boundary in the H-R diagram. The upper star indicates the position of 41 Cyg (F5 II); the lower one α CMi (F5 IV–V).

As can be seen from Table 1, the signal-to-noise ratios generally exceed 500. Bisector errors arise mainly from spectrophotometric errors divided by the slope of the profile (see Gray 1983) and, therefore, are larger near the top and bottom of a bisector. It is very difficult to follow the bisectors higher than about 95% of the continuum. Figures 2 and 3 show examples of the level of consistency obtained from these observations. The agreement among the exposures is excellent, and there is no evidence of temporal variability. Mean bisectors were therefore constructed for each line by combining the bisectors from the different exposures. They are discussed next. Recall that absolute wavelength shifts of stellar line bisectors cannot be measured because of the arbitrary radial velocity of the stars.

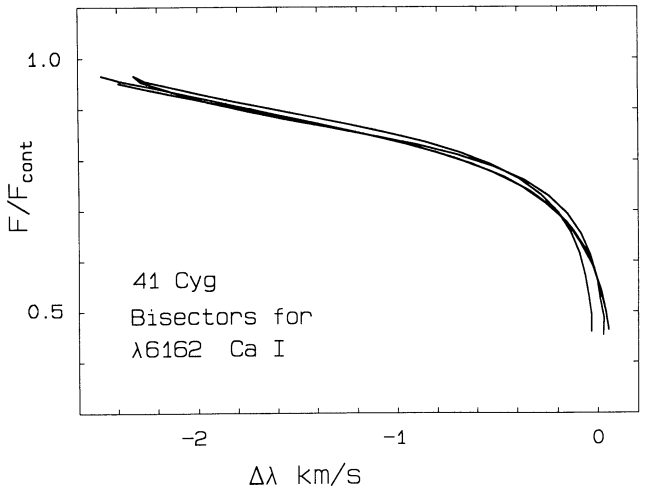

FIG. 2–Four exposures (see Table 1) yield these spectral-line bisectors for Ca I λ6162.18. The zero point of the velocity scale is arbitrary.

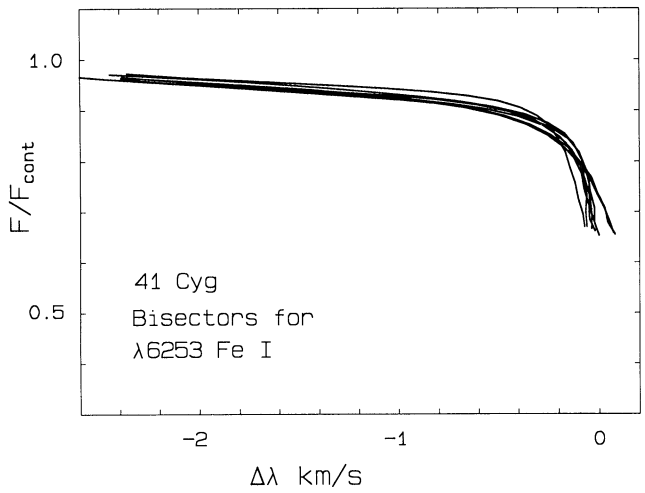

FIG. 3–Eight exposures (see Table 1) yield these spectral-line bisectors for Fe I λ6252.57. The zero point of the velocity scale is arbitrary. The most discordant bisector comes from the exposure having the lowest signal-to-noise ratio.

3. The Observed Line Bisectors

In past studies I emphasized how line bisectors from all strength lines can be combined into a coherent composite plot, leading to a mean bisector for a given star. This behavior is reiterated here with α CMi in Figure 4. Bisector means are computed for groups of lines having similar strength, and they are shown on the left-hand side of the figure. They are then shifted horizontally and aligned by eye to form the composite on the right-hand side. As can be seen, all five of these mean bisectors appear to map out one unique shape—a grand mean bisector for the star. The deviations in the composite amount to only $\sim \pm 10$ m s^{-1} and are of the order of the expected errors of measurement. This is not to say that second-order differences associated with different ions,

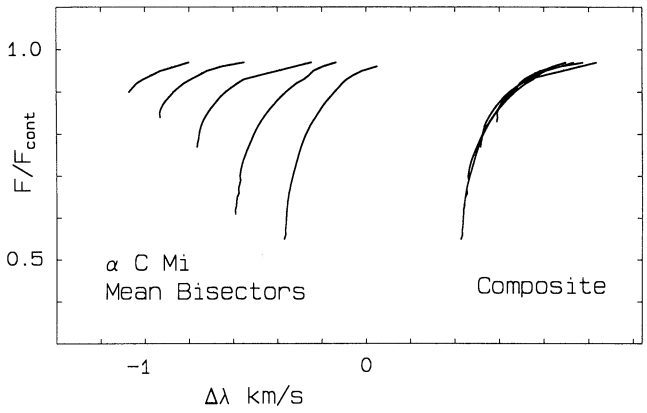

FIG. 4–The left-hand portion shows mean bisectors for small groups of lines having similar strength (λ6141.72, λ6161.18, λ6122.23; λ6230.74, λ6252.57, λ6246.33; λ6219.29, λ6149.25, λ6256.37, λ6265.14, λ6232.65; λ6166.44, λ6245.20; λ6165.36, λ6258.11). They are positioned arbitrarily along the velocity coordinate. The right-hand part of the diagram show these same bisectors shifted along the velocity coordinate to illustrate the identical shape each has and how a composite for the star can be formed.

different excitation potential, widely different wavelength regions, etc., will not eventually be measured. But these particular lines are sufficiently homogeneous in such parameters to show a consistent bisector shape. Notice specifically how the weaker lines show bisectors that look like the top portion of bisectors for stronger lines. Whatever the reason for this, the bisectors for stars on the cool side of the granulation boundary fit together to delineate one mean bisector for that star.

The behavior for the hot stars is very different, as shown in Figure 5. Notice the much larger velocity span for these reversed bisectors compared to those of cool stars (e.g., Fig. 4). Figure 5 also shows how each line produces the *full* reversed bisector. Specifically, the weaker lines do not just look like the tops of bisectors for the stronger lines. Instead, they show the whole shape, including the near-vertical portion at the bottom. Clearly it is inappropriate to form a composite and mean bisector, as has been done for cool stars. Instead, the hot-star bisectors are normalized by the central depth of the line. Actually I used twice the central depth in order to make the results more visually compatible to the usual plots of bisectors. Now we see in Figure 6 much closer agreement among the bisectors, although a small but significant systematic dependence on line strength remains which is, as I will show below, a result of the different blurring caused by the different widths of the thermal profiles. In other words, the macroscopic velocity field in hot stars leaves a complete and identical signature on each line profile.

4. Numerical Simulations: Concepts

I use here a kinematic two-stream "model" to do some

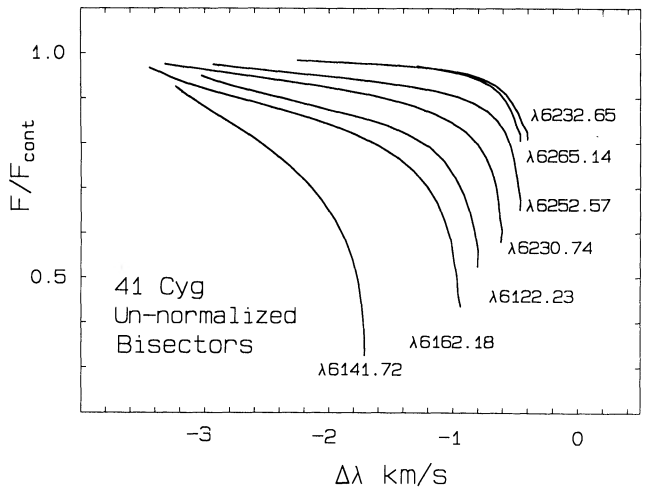

FIG. 5–The line bisectors for seven lines in 41 Cyg are shown. The velocity zero point is arbitrary. Each bisector shows a quasi-vertical portion corresponding to the cores of the lines and a broadly sweeping blueward portion from the wings of the lines.

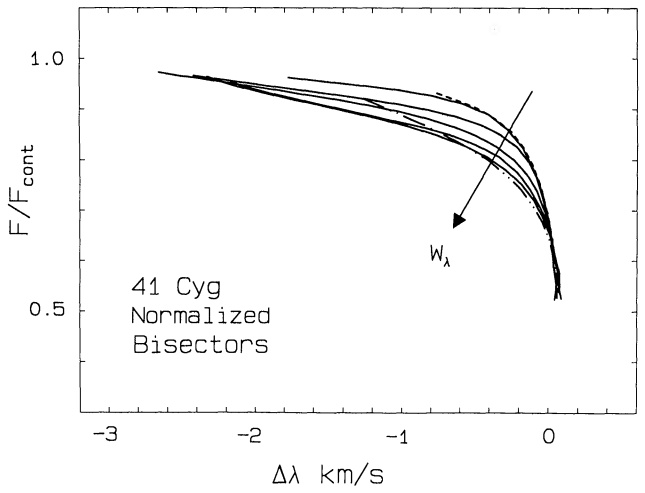

FIG. 6–Scaling the bisectors to (twice) the line depth results in this diagram. The bisectors are now much more nearly the same but show a change with increasing equivalent width of the line, W_λ, in the sense indicated by the arrow.

numerical simulations. No attempt is made to include hydrodynamical physics. For such calculations one should refer to Dravins and Nordlund (1989), Nordlund (1982), Atroshchenko, Gadun, and Kostik (1989), Gigas (1989), and Steffen (1989). No hydrodynamical calculations are available for stars like 41 Cyg. The simulations used here are similar to those used earlier (Gray and Toner 1985). As pointed out in the Introduction, the anisotropic nature of the velocity fields is the key property to be mimicked by the calculations. Two of the following three streams were included in a simulation: (1) a hot stream with vertical velocities (only) having a (non-isotropic!) Gaussian distribution with dispersion ζ around a mean v_h, (2) a similar cold stream having vertical velocities of dispersion ζ around a mean v_c, or (3) a "neutral" stream having isotropically oriented velocities of Gaussian dispersion ζ. The dispersion was taken to be the same for both streams. All parameters are single values; no depth dependences are included. The orientation of the velocity vectors is very important. Vertical velocities produce decreasing Doppler shifts from the center of the disk to the limb. Likewise their *distributions* around the mean velocities become narrower toward the limb. The neutral stream is intended to represent material lying between the stream structure and is therefore chosen to have an isotropic velocity field. In all models, the hot-stream velocities are anisotropic, specifically, vertical. In addition to these Doppler shifts, those of rotation are also included. The full Doppler-shift distribution is obtained by integrating the apparent stellar disk in a radius-annulus format. Typically 8000 to 10,000 small disk areas enter the final integration. The adequacy of the fineness of the grid is ascertained by computing a series of disk integrations with progressively finer integration steps until any changes are obviously smaller than the observational errors.

Since the thermal line profile is usually narrow compared to the Doppler shifts of the macroscopic velocity fields, its primary function is as a marker of Doppler shifts. The strength of the continuum is, therefore, the more basic photometric parameter, not the strength of the line. In each small disk area, the continuum strengths are set by the limb darkening, given by $I/I_0 = 0.6 - 0.4 \cos\theta$, and the amount of light coming from the streams, denoted by F_h, F_c, and F_n. Each fractional photon flux, such as F_h for the hot stream, is physically controlled by the combined effects of specific intensity and the time-averaged fractional area covered by that stream. Without resorting to second-order effects, there is no way to separate these two factors, and I make no attempt to separate them here. The secondary effect of the thermal profile is the smearing it introduces—it is not negligibly narrow compared to the macrovelocities. To approximately allow for this smearing, the disk-integrated Doppler-shift distribution is convolved with a thermal profile computed from an LTE model photosphere. These thermal profiles are chosen to match the equivalent widths of the observed lines, and the atomic parameters of the observed lines are used in the calculations.

5. Numerical Simulations of Reversed Bisectors

Reversed bisectors can be simulated with both one- and two-stream models. The mechanism giving the reversed shape is basically different in the two cases. A one-stream model having a single rising stream relies on the "expanding-star effect" (Gray and Toner 1985) in which the small Doppler shifts from the large limb area combine with the large Doppler shifts from the small

central area to produce the appropriate tail on the disk-integrated Doppler-shift distribution. The return stream is postulated to be too faint to sensibly affect the spectrum. Two-stream models, by contrast, produce asymmetries by having the streams positioned appropriately on the velocity coordinate and, of course, they must contribute unequal numbers of photons to the integrated spectrum. The extra parameters of the two-stream models allow more details of bisector shape to be matched.

A single stream was used to model the reversed bisectors of γ Cygni (Gray and Toner 1986). At that time we did not realize the morphological differences between the bisectors of cool and hot stars, and all the observed bisectors were placed in a composite plot without normalization to the depth of the line. Although the single-stream modeling gave passably good agreement with this erroneously assembled composite, it was not perfect. In particular, the dispersion had to be large, $\zeta \approx 9$–10 km s^{-1} with $v_h \approx -25$ km s^{-1}, to get the proper bisector shape, and this made the simulated *profiles* somewhat wider than the observed ones. Now, with better understanding of the morphology and with the better-quality 41 Cyg data, I find the one-stream model is no longer adequate.

Two-stream simulations give considerably better agreement with both the bisectors and the profiles. Only a few combinations of parameters yield acceptable results, however. In general the rising stream must contribute a small part, $\approx 10\%$, of the integrated spectrum, and the rise velocity must be large, $v_h \approx -10$ to -20 km s^{-1}. Constraints on the dominant second stream are much weaker. For example, a neutral stream (isotropic velocities), where the average velocity is zero, can be replaced by a falling stream (nonisotropic velocities), where the stream velocity is less than $\sim +5$ km s^{-1}, to give equally good agreement with the observations.

According to the evidence in Section 3, the same macrovelocity field shapes all strength lines. I therefore selected one line, λ6162.18, and searched for two-stream model parameters giving acceptable agreement with it. It is reasonably easy to obtain rather good agreement with the bisector alone. One case has $v_h = -13.0$ km/s, $F_h = 0.2$, $F_n = 0.8$, $\zeta = 3.0$, and $v \sin i = 5.0$, to be specific. The observed mean bisector is matched to about one-tenth of the scatter seen in Figure 2. There are many combinations of parameters that fail even this minimal constraint. In other words, the detailed bisector shape alone contains a great deal of information. But this model fails because it produces a profile about 3% too deep in the core with correspondingly too narrow dimensions toward the shoulders of the profile. And, in fact, when the constraints of the line profile are added to those of the bisector, it is rather difficult to find satisfactory two-stream solutions. Specifically, the velocity span and slope of the top portion of the bisector are sensitive to v_h and F_h. The shape of the profile is most sensitive to ζ and $v \sin i$. Quite generally the relatively sharp curvature of the bisector hardly allows ζ and $v \sin i$ to be large enough to supply the broadening needed in the profile. An example of a rising-plus-neutral stream match is given in Figure 7. The agreement is acceptably good even though small systematic differences can still be seen. Equally good models for λ6162.18 can be found with the neutral stream replaced by a slowly falling cold stream. In such cases, the difference between v_h and v_c is approximately conserved. The most direct way to establish v_c would be to use observations of absolute velocity displacements for the line bisectors which, of course, are not available.

There is also ambiguity between $v \sin i$ and ζ. One can be traded against the other, to a limited degree, to maintain acceptable agreement for both the bisector and the profile. (The acceptable rotation rates are too small compared to the linewidths to show a sensible "rotation effect", i.e., an enhancement of asymmetry by rotation. See Gray 1986*b*; Smith, Huang, and Livingston 1987.) Resolution of this ambiguity is supplied by the other spectral lines. In particular, if ζ is chosen too large at the expense of $v \sin i$ when λ6162.18 is modeled, the weaker lines then show more asymmetry than observed. Imbalances of ζ and $v \sin i \sim 2$ km s^{-1} can be detected with the seven lines being used.

Figure 8 shows the calculated counterpart of Figure 6 for the solution illustrated in Figure 7. The basic dependence on equivalent width is reproduced. Individual line-by-line bisector comparisons are shown in Figure 9. The line profiles, which are not shown in Figure 9, do not show any systematic disagreements as a function of line strength, but some of the individual profiles show noticeably less good agreement than for λ6162.18 (Fig. 7). The poorest agreement is seen for the strongest line, λ6141.72, where the influence of the thermal profile is greatest. No doubt this stems from the approximate treat-

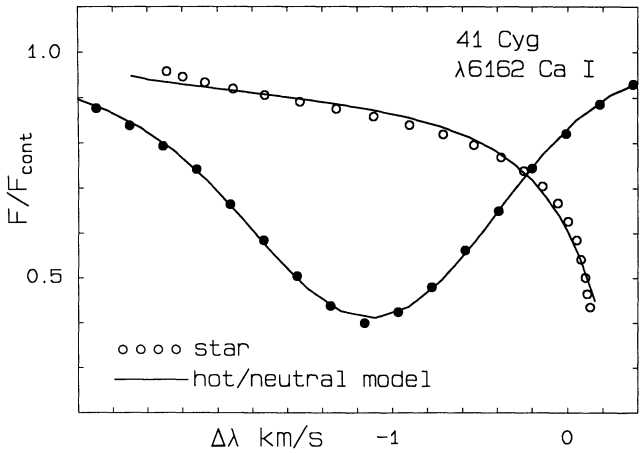

FIG. 7–The two-stream model having $v_h = -17.0$, $F_h = 0.12$, $F_n = 0.88$, $\zeta = 4.0$, and $v \sin i = 7.0$ gives an acceptably good solution for both the bisector and the profile. The shown velocity scale is for the bisector; the scale for the profile is compressed ten times.

ment of the thermal profile in the modeling. It may be that fine adjustment of model parameters might lead to an even better agreement, but we must bear in mind the crudeness of the two-stream calculations and not waste too much effort tuning meaningless details.

6. Comments

The classical bisector shapes of cool stars are quite generally understandable in terms of a granulation-type velocity field in which the rising elements contribute more photons than the falling ones do. Solar observations also tell us the rising material is hotter, that most of the bisector is blueshifted, and that we are dealing with a convection-induced phenomenon. For the hot stars, those on the hot side of the granulation boundary, we have no solar counterpart. We deduce from the best-fitting two-stream models that the rising material contributes ~ 10% of the light, and naturally we are likely to argue that the material is rising because it is hotter, presuming that convection is the driver of the motions. If the rising material is hotter, then we would deduce its fractional area to be even less than ~ 10%. We might imagine geyser-like plumes, or a forest of widely spaced "tree trunks", into which the upward-moving streams are localized.

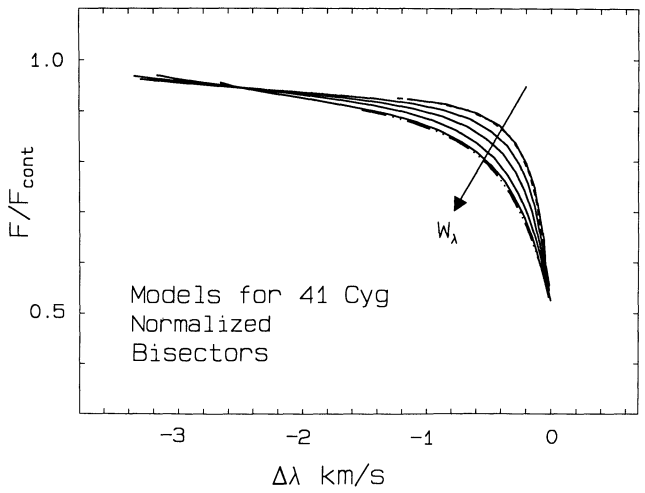

FIG. 8–The solution given in Figure 7 is also an acceptable solution for the lines of other strength, and dependence on equivalent width mimics the observations displayed in Figure 6.

Another factor may be equally important—the factor of time. The observations tell us the *time-averaged* fractions of photons contributed by the rising stream is small, not the area as such. Suppose very large-area "bubbles" rise through the photosphere sporadically and for only a small fraction of the time. Numerous such bubbles distributed across the stellar disk would preclude observable time variations. But, unlike the solar case, we might imagine most of the hot-star photosphere to be quiescent most of the time with occasional bubbles bursting forth. Terrestrial analogies are seen in the bubbling of "mud pots" and "hot springs" in areas of geothermal activity.

The scaling properties of bisectors for hot and cool stars (Fig. 4 vs. Fig. 6) are also very different. How might we account for this? Cool-star granulation is depth dependent. How deeply we see into the granulation depends on the opacity. A weak line hardly increases the absorption coefficient above the continuous absorption and so weak lines are formed deep; their shapes tell us about the Doppler-shift distribution relatively deep down in the photosphere. The same can be said for the *wings* of strong

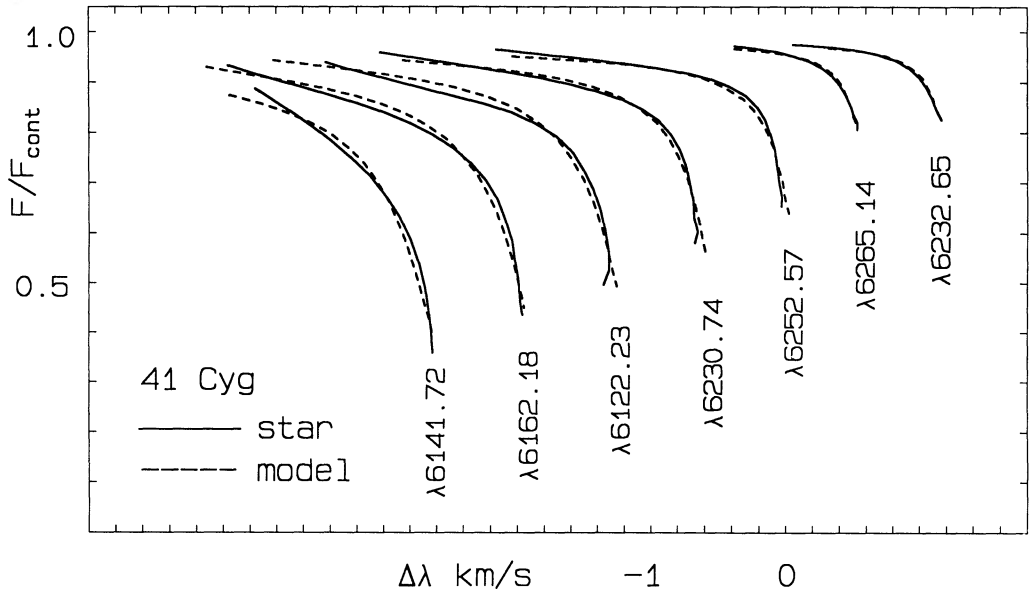

FIG. 9–The unnormalized bisectors from the hot/neutral-stream model (see Fig. 7) are compared to the observations. The agreement is reasonable, although small systematic discrepancies can be seen.

lines. So it is not surprising, then, to find the bisectors of weak lines and the tops of bisectors for strong lines showing similar shapes. Granulation loses its vigor with height. If the core of a strong line is sufficiently deep, the effective level of formation will be at high layers in the photosphere. The bisector for the core of a strong line will reflect the vigor of the granulation at these higher layers. Composite bisectors, like the one in Figure 4, can be made because the depth dependence of the granulation is automatically probed according to the amount of absorption occurring at each depth in a spectral line. To first order, equal absorption levels (or bisector points), irrespective of whether the point is in a weaker or a stronger line, reflect the Doppler shifts at the same depth. Naturally, second-order effects arising from line-to-line differences in excitation potential, ionic species, etc. will exist. We are not yet able to measure these differences in stars generally.

Following this line of thinking, the natural explanation of the behavior for hot-star bisectors is the *lack* of any depth dependence in the velocity field. This could occur if the stellar surface were optically very thick or if the differential motions within a stream were simply very small throughout the line-forming layers. This may seem unlikely for a star of such low surface gravity but perhaps not if either geyser-like structures or large sporadic bubbles are involved.

Theoretical studies of thin convection zones for the hot stars are badly needed. Extending the observations to still hotter stars might help establish the convective nature of the velocities (or otherwise), since the calculations claim that a drop in velocities will eventually occur for sufficiently high effective temperatures as the hydrogen and then the helium ionization zones disappear.

The lack of time variability in these bisectors implies not only the lack of significant pulsation-type variability but also the lack of surface features such as starspots and starpatches (Toner and Gray 1988).

I wish to acknowledge the help of C. G. Toner, Y. Cheng, T. Kennelly, C. Boyd, and S. Butterworth in acquiring some of the data used here. Stimulating discussions with several members of the Department of Astronomy at Yale University helped improve this study. I am grateful to the Natural Sciences and Engineering Research Council of Canada for financial support.

REFERENCES

Atroshchenko, I. N., Gadun, A. S., and Kostik, R. I. 1989, *Solar and Stellar Granulation*, ed. R. J. Rutten and G. Severino, (Kluwer: Dordrecht), p. 135.
Cox, J. P., and Giuli, T. R. 1968, *Principles of Stellar Structure* (New York: Gordon and Breach).
Dravins, D. 1982, *Ann. Rev. Astr. Ap.*, **20**, 61.
———. 1989, *Solar and Stellar Granulation*, ed. R. J. Rutten and G. Severino (Kluwer: Dordrecht), p. 493.
Dravins, D., and Nordlund, A. 1989, *Astr. Ap.*, submitted.
Gigas, D. 1989, in *Solar and Stellar Granulation*, ed. R. J. Rutten and G. Severino (Kluwer: Dordrecht), p. 533.
Gray, D. F. 1976, *The Observation and Analysis of Stellar Photospheres* (New York: Wiley).
———. 1982, *Ap. J.*, **255**, 200.
———. 1983, *Pub. A.S.P.*, **95**, 252.
———. 1986*a*, in *IAU Symposium 118, Instrumentation and Research Programmes for Small Telescopes*, ed. J. B. Hearnshaw and P. L. Cottrell (Dordrecht: Reidel), p. 401.
———. 1986*b*, *Pub. A.S.P.*, **98**, 319.
———. 1988, *Lectures on Spectral-Line Analysis: F, G, and K Star* (Arva, ON: The Publisher).
Gray, D. F., and Cheng, Y. 1989, in preparation.
Gray, D. F., and Nagel, T. 1989, *Ap. J.*, **341**, 421.
Gray, D. F., and Toner, C. G. 1985, *Pub. A.S.P.*, **97**, 543.
———. 1986, *Pub. A.S.P.*, **98**, 499.
Hill, G. 1982, *Pub. Dom. Ap. Obs.*, **16**, 67.
Nordland, A. 1982, *Astr. Ap.*, **107**, 1.
Renzini, A., Cacciari, C., Ulmschneider, P., and Schmitz, F. 1977, *Astr. Ap.*, **61**, 39.
Rutten, R. J., and Severino, G., eds. 1989, *Solar and Stellar Granulation* (Dordrecht: Kluwer).
Schroter, E. H. 1957, *Zs. f. Ap.*, **41**, 141.
Smith, M. A., Huang, Y. R., and Livingston, W. 1987, *Pub. A.S.P.*, **98**, 297.
Steffen, M. 1989, in *Solar and Stellar Granulation*, ed. R. J. Rutten and G. Severino (Dordrecht: Kluwer), p. 425.
Toner, C. G., and Gray, D. F. 1988, *Ap. J.*, **334**, 1008.
Voigt, H. H. 1956, *Zs. f. Ap.*, **40**, 157.
———. 1958, *Zs. f. Ap.*, **47**, 144.